ELSEVIER

Int. J. Therm. Sci. 41 (2002) 332–340

International Journal of Thermal Sciences

www.elsevier.com/locate/ijts

Convective heat transfer in a channel with perforated ribs

Transfert de chaleur par convection dans un canal muni de pontets perforés

Jean-Marie Buchlin

Von Karman Institute for Fluid Dynamics, Environmental and Applied Fluid Dynamics Department, Chaussée de Waterloo, 72, B-1640 Rhode Saint Genèse, Belgium

Received 24 July 2001; accepted 30 October 2001

Abstract

An experimental study of convective heat transfer in a channel implemented with perforated ribs immersed in a turbulent boundary layer is presented. Infrared thermography associated with the steady heated thin foil technique is applied to obtain the mapping of the heat transfer coefficient. Different types of perforations are compared in the case of single turbulator configuration. Conclusions are drawn on the effect of the rib design on the heat transfer enhancement. Next, the study focuses on the turbulator with perforations of chevron type. Then, emphasis is given to the influence of the rib-to-rib spacing, the open-area factor and the channel Reynolds number on the thermal exchange. Compared to solid rib, a local thermal enhancement factor of 3 can be expected just behind the perforated turbulator. Fully developed flow is reached after the 5th to 6th rib. The optimal design combines a rib pitch ratio of 5 with an open area factor of 0.53 for channel Reynolds number ranging from 30000 to 60000. © 2002 Éditions scientifiques et médicales Elsevier SAS. All rights reserved.

Résumé

Le papier décrit une étude expérimentale du transfert de chaleur par convection forcée dans un canal muni de pontets perforés immergés dans une couche limite turbulente. La thermographie infrarouge est combinée à la technique stationnaire du feuillet chauffant pour obtenir la cartographie du coefficient de transfert de chaleur. Différents types de perforation sont comparés dans le cas d'une configuration à un turbulateur. Des conclusions sont tirées quant à l'effet de la forme du pontet sur l'amélioration du transfert de chaleur. Par la suite, l'étude se consacre au turbulateur avec des perforations à chevron. L'accent est alors placé sur l'influence de l'espacement entre pontets, de la porosité de surface du pontet et du nombre de Reynolds du canal sur l'échange thermique. Comparé au pontet plein, une amélioration du nombre de Nusselt local d'un facteur 3 peut être obtenue juste en aval d'un turbulateur perforé. Le régime développé est atteint après 5 à 6 pontets. Un arrangement optimal se dessine pour un rapport espacement/hauteur de 5 avec une porosité de surface de 0,53 dans la plage du nombre Reynolds du canal de 30000 à 60000. © 2002 Éditions scientifiques et médicales Elsevier SAS. All rights reserved.

Keywords: Convective heat transfer enhancement; Perforated turbulators; IR thermography

Mots-clés : Amélioration de transfert de chaleur par convection forcée ; Turbulateurs perforés ; Thermographie infrarouge

1. Introduction

Turbulent flows around bluff bodies are characterised by the formation of complex vortical regions that govern the thermohydraulic behaviour of the system [1]. The presence of ribs, represented by prismatic obstacles emerging from a flat wall in a turbulent boundary layer, produces typical flow pattern which is encountered in many engineering situations such as heat exchangers, advanced gas-cooled reactor fuel elements, blade internal cooling channels, ventilation equipment of microelectronics systems. The ribs, which are generally of solid type, create local wall turbulence due to the separation and reattachment of the flow. However, in addition to pressure drop penalty, the solid turbulators induce local heat transfer deterioration and subsequent hot spot formation at

E-mail address: buchlin@vki.ac.be (J.-M. Buchlin).

1290-0729/02/$ – see front matter © 2002 Éditions scientifiques et médicales Elsevier SAS. All rights reserved.
PII: S1290-0729(02)01323-6

Nomenclature

e	thickness of the heated plate	m
EF_h	thermal enhancement factor	
h	heat transfer coefficient	$W{\cdot}m^{-2}{\cdot}K^{-1}$
H	height of the rib	m
k	thermal conductivity	$W{\cdot}m^{-1}{\cdot}K^{-1}$
q	heat flux	$W{\cdot}m^{-2}$
Nu	Nusselt number based on channel height	
Nu_H	Nusselt number based on H	
$\langle Nu_H \rangle$	mean Nusselt number	
Nu_o	Nusselt number without rib	
P	spacing between two successive ribs	m
Re	channel Reynolds number	
Re_H	Reynolds number based on H	
T	temperature	K
TU	IR thermal unit	
U	velocity	$m{\cdot}s^{-1}$
x	axial co-ordinate	m
y	spanwise co-ordinate	m

Greek symbols

β	open area factor	
ν	kinematic viscosity	$m^2{\cdot}s^{-1}$

Subscript

c	convection
H	based on rib height
f	air
j	Joule
ℓ	conductive and radiative heat losses
r	radiant contribution
w	wall
∞	free stream

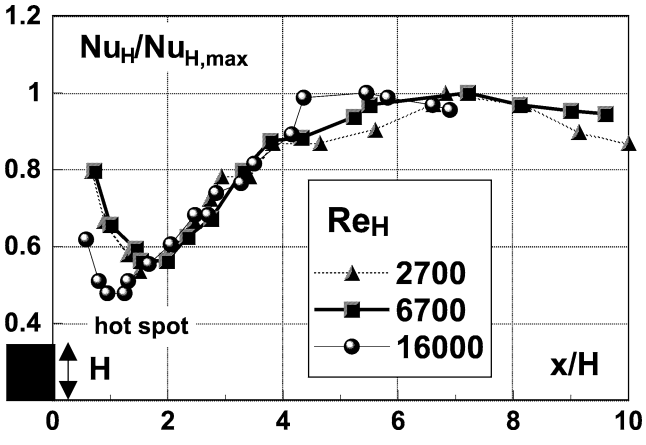

Fig. 1. Heat transfer distribution behind solid-type turbulator [2].

their rear concave corner as shown in Fig. 1 [2]. To get rid of this deficiency, turbulent porous or perforated turbulence promoters have been proposed [3]. So far, most of the perforations tested consist of rows of holes drilled trough the ribs [4–6]. The heat transfer coefficient is generally determined by temperature measurements performed by thermocouples flush-mounted on a heated wall and/or laser holographic interferometry to retrieve the thermal boundary layer profile [7,8].

This study focuses on the heat transfer enhancement achieved with new designs of perforated turbulator. Tests are conducted on a single and multiple two-dimensional rectangular and thermally passive ribs (unheated) placed in a turbulent boundary layer that develops over a heated flat plate. The experimental method involves the steady state measurement of the wall temperature by means of an infrared scanning radiometer.

2. Experimental method

The convective heat transfer behind the rectangular perforated rib mounted on the flat plate is studied by means of the thermofoil technique previously developed at the von Karman Institute to investigate heat transfer of impinging jets [9,10]. The wall is designed to dissipate by Joule effect a constant (in time) and uniform (in space) heat flux q_j. The measurement of the steady state distribution of the surface temperature $T_w(x, y)$ allows the determination of the local convective heat transfer coefficient $h_c(x, y)$ according to the Newton relation:

$$h_c = \frac{q_j - q_\ell(x, y)}{T_w(x, y) - T_f} \tag{1}$$

In the above expression, T_f is the free stream temperature and q_ℓ is the heat loss by conduction in the plate and radiation between the wall and the surrounding. Assuming all the environment at the fluid temperature, h_c can be expressed making use of the fin theory:

$$h_c = \frac{q_j + e \cdot k \cdot \nabla^2 T_w}{T_w(x, y) - T_f} - h_r \tag{2}$$

e and k are the thickness and the thermal conductivity of the plate, respectively. The radiative heat transfer coefficient, h_r, is estimated by means of the radiosity concept once T_w is known. Eq. (2) leads to the following recommendations: the heated plate should be of low thermal conductivity and small thickness and/or the thermal sensor should have a high spatial resolution to resolve properly the conductive term; it should be uniformly covered with coating of large emissivity to avoid artificial distortion in the temperature field and difficult reflectivity corrections. In this respect, infrared thermography is an appealing technique.

3. Experimental test set-up

The experimental investigation is carried out in the VKI-L12 wind-tunnel. The facility is sketched in Fig. 2. A close view of the test section is shown in Fig. 3. The test section is 0.2×0.2 m^2 in cross section and 1.5 m long. A maximum free stream velocity U_∞ of 25 m·s^{-1} with a turbulence level of 0.3% can be attained. A hot wire anemometer or a Pitot tube fixed to a displacement mechanism and connected to a pressure transducer is used to measure the velocity profile through the boundary layer.

The heating device is a serpentine-shaped copper thermofoil resistance (16 Ω) sandwiched between two thin black painted Bakelite plates of 1.5 mm thick and of low conductivity (0.15 W·m^{-1}·K^{-1}). This flat heater, 1.25 m long and 0.2 m wide, is fixed at the centre of the test section and produces a uniform and equal heat flux on both sides. The resulting square-wave continuous electrical resistance is connected to an AC generator. The Joule heating is monitored by potentiometer, ammeter and voltmeter. A maximum heat flux of 3000 W·m^{-2} can be achieved; however, the wall temperature has to be limited to 80 °C to ensure the integrity of the set-up. Both faces of the heated flat plate are coated with a black paint of emissivity factor $\varepsilon_w = 0.95$ to improve the thermography measurements and allow correction for radiation.

Five types of perforated rib turbulator, 20 mm high and 20 mm wide, made in Plexiglas are tested. They are sketched in Fig. 4. The channel blockage does not exceed 20%. The

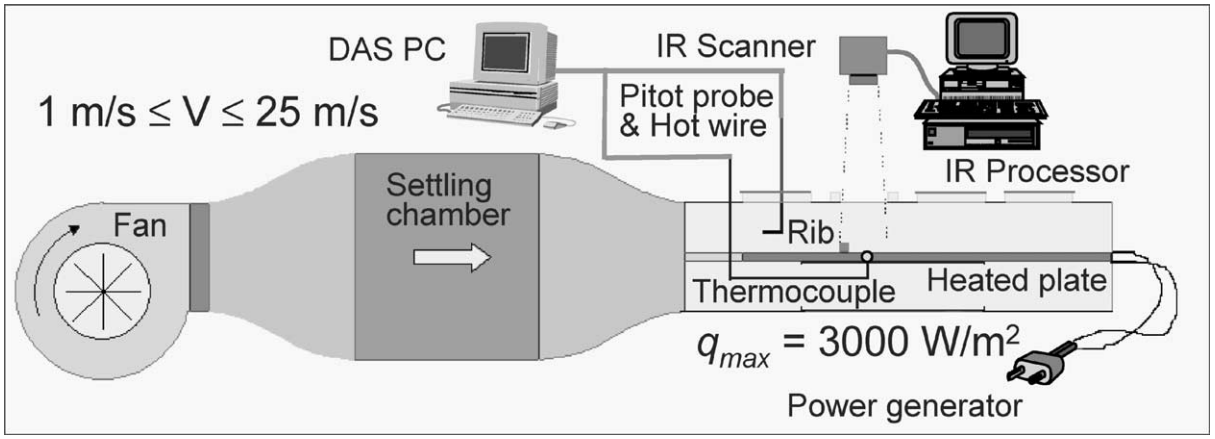

Fig. 2. Schematic of the test facility VKI-L12.

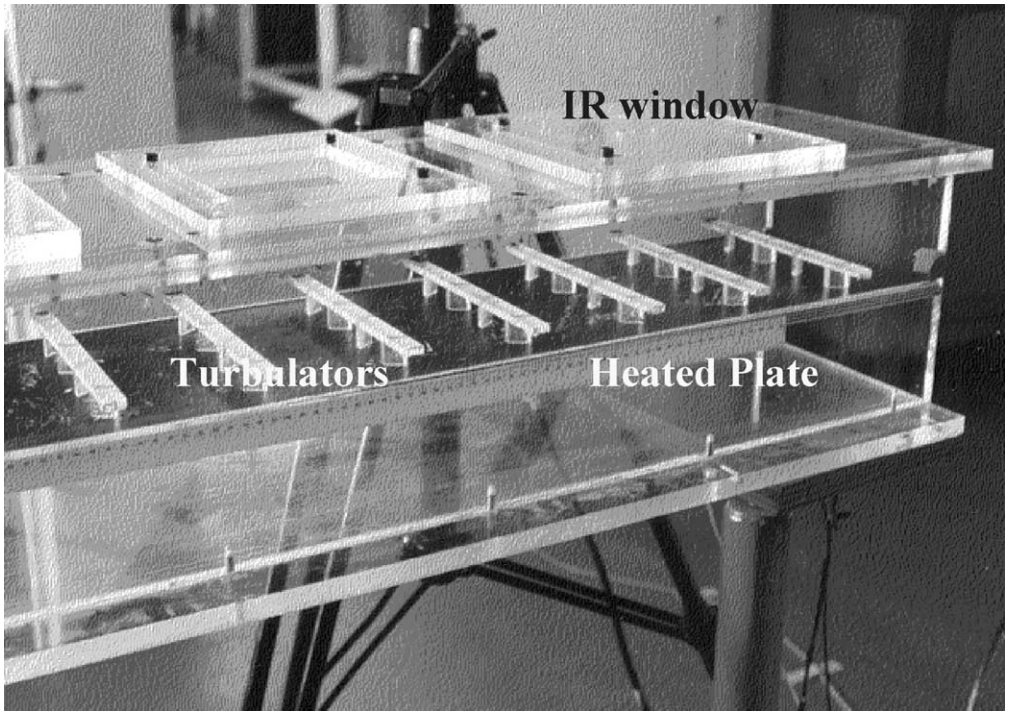

Fig. 3. Close view of the test section.

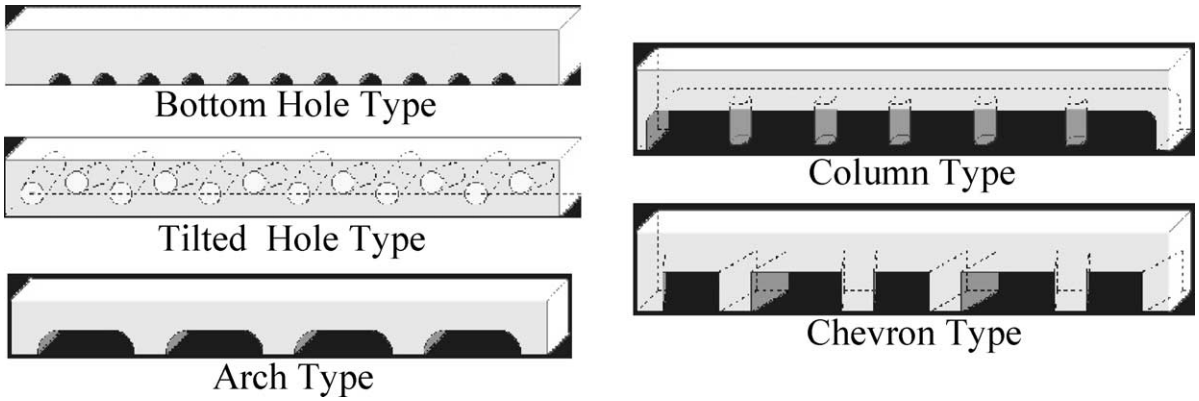

Fig. 4. Schematic of the perforated turbulators tested.

first type is composed of 8 half holes of 8 mm in diameter, horizontally drilled on the base of the rib (BH-type). The second promoter of is perforated by a raw of 12 holes, 8 mm in diameter, alternatively tilted upward and downward (TH-type). Four arches of 9 mm in height and 34 mm in width form the third turbulator (AR-type). The arches are replaced by 5 columns made of small cylinders of 5 mm in diameter and 15 mm high to obtain the fourth obstacle (CO-type). Finally, the last permeable rib is composed of chevron shape clearances corresponding to 5 alternate diverging and converging apertures, 15 mm high and 20 mm wide for the larger section, with a total opening angle of 40° (CH-type). Preliminary tests have shown that the same heat transfer coefficients are obtained when identical ribs are placed symmetrically on each face of the heated wall or when they are only located on the top face. Therefore, all the tests are conducted with only turbulators placed on the upper face of the flat plate.

The IR radiometer is the AGEMA Thermovision 900 system with a HgCdTe detector sensitive in the 8–12 μm wavelength range and cooled by liquid nitrogen. The measurable temperature range is −30 °C to 1500 °C with an announced thermal sensitivity of 0.1 °C. The camera is equipped with a standard optical set-up of (10° vertical) × (5° horizontal) giving an instantaneous field of view (IFOV) of 0.76 mrad. The camera scans an area of about 80 × 80 mm^2 located behind the obstacle, via a special 45-degrees mirror and through a transparent plastic window. It is connected to a dedicated PC for acquisition at a frame rate of 20 Hz and processing of thermograms (272 × 136 pixels). The thermography system is calibrated prior to each test by means of T-type thermocouples flush-mounted on the top face of the heated plate and connected to a PC-controlled data acquisition system. A typical calibration curved is plotted in Fig. 5. The thermography system is calibrated prior to each test by means of T-type thermocouples flush-mounted on the top face of the heated plate and connected to a PC-controlled data acquisition system. Linear fit models satisfactorily the relation between the radiometer output, in terms of the thermal unit TU, and the wall temperature T_w for the test conditions herein considered. Data reduction indicates that the thermal losses by conduction remain negligible since they do not exceed 2%, while the heat losses by radiation can add up to 13% of the total flux.

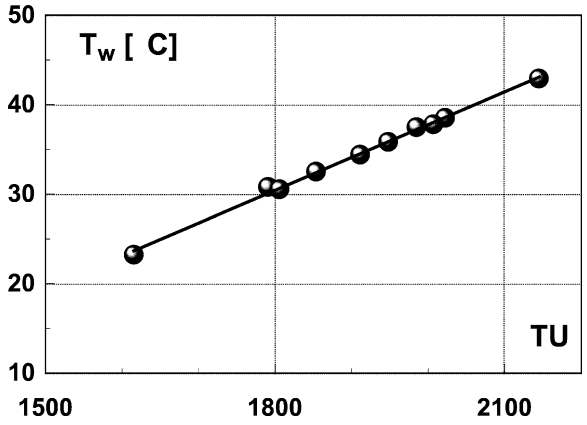

Fig. 5. Calibration curve of the IR radiometer.

4. Typical results

4.1. Single rib configuration

Tests have been carried out for rib Reynolds numbers, based on rib height H and unperturbed free-stream velocity U_∞, ranging from 5000 to 35000. The convective heat transfer coefficient is represented by the Nusselt number $Nu_H = h_c H / k_f$ where k_f is the air thermal conductivity.

Typical mapping of the Nusselt number behind each type of turbulator is shown in the layout of Fig. 6 for rib Reynolds number equal to 22000. Each rib design produces a different heat transfer mapping which reflects the footprint of the flow pattern and the turbulence features associated with.

The BH-type rib gives rise to the formation of a multi wall-jet system, the strength of which decreases quickly so that no more effect is appreciated at a downstream distance $x \approx H$. From this location no significant spanwise variation of Nu_H is observed indicating that the flow has retrieved its two-dimensional character. A minimum heat

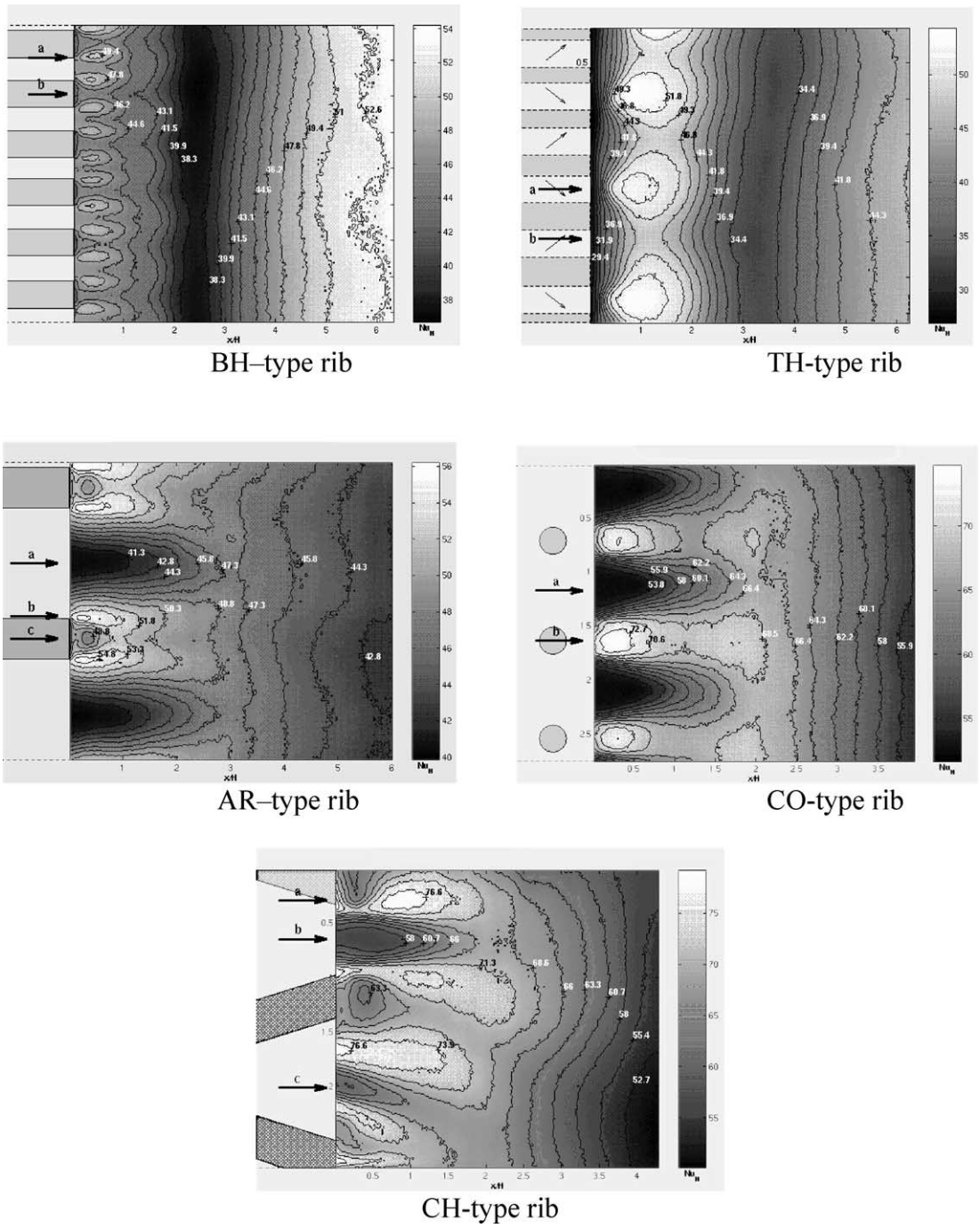

Fig. 6. Mapping of the heat transfer coefficient: $Re_H = 22000$.

transfer coefficient is found at $x \approx 2H$ where local flow detachment occurs due to the impact of the wall jets onto the recirculation bubble provoked by the upper-flow impingement ($x > 6H$).

The Nu_H-mapping of the TH-type rib reveals the presence of high Nu_H-values, which results from local impinging jets exhausting from the holes tilted downward. An area of strong convection, about $2.5H$ width, is thus realised and delays the minimum heat transfer ($x \approx 3H$) compared with the BH-configuration.

The other perforated rib designs yield unanticipated findings. The mapping corresponding to AR-type as well the CO-type turbulators point out that zones of high heat transfer appear in the wakes of the arch pylons or the cylindrical columns but not in the continuation of the clearance where paradoxically low values of heat transfer coefficient are observed. These Nu_H-distributions hint at the formation of complex vortical three-dimensional structures produced by the interaction of the upper flow with the wakes leading to area dominated by high turbulence level. However, it

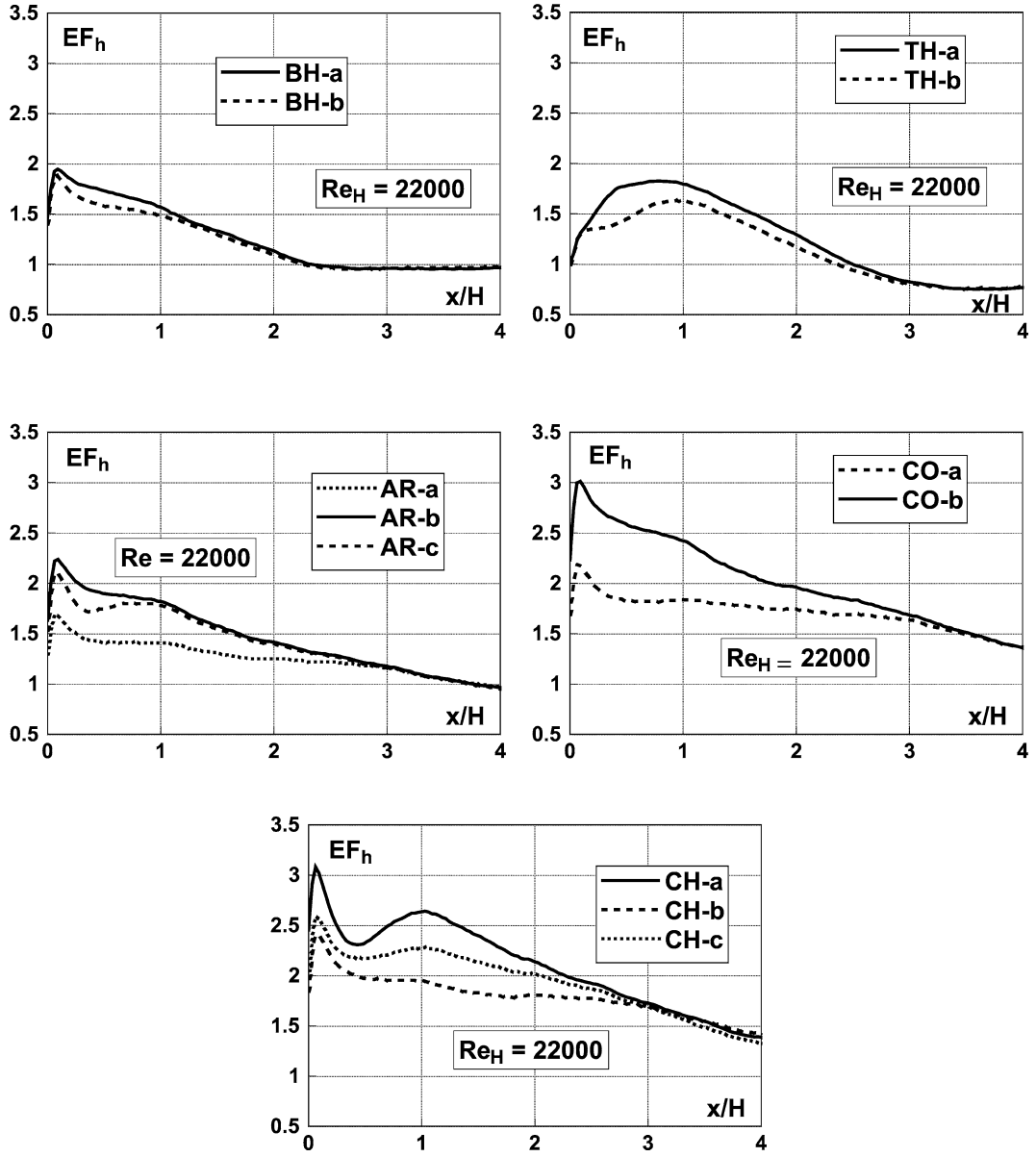

Fig. 7. Downwind distribution of the enhancement factor.

is worth noticing that the distribution remains rather well organised in the spanwise direction.

Although the same trends are depicted on the Nu_H-mapping of the CH-type rib, additional peculiarities have to be emphasised. A spanwise distortion is now noticeable. It is mainly due to the development of a lower-heat-transfer region at the exit of the converging section whereas the diverging opening provides good thermal exchange. This is particularly noticed at the edges where vortices are probably generated by the flow detachment inside the diverging perforation. In such a condition, it is conceivable to suspect the presence of an unsteady or oscillatory flow pattern resulting from interactions between the different streams. Unfortunately, such an information cannot be conveyed by the heat transfer data given the thermal inertia of the heated plate. Therefore, complementary aerolic measurements should be performed to confirm such a behaviour.

To quantify the thermal enhancement provided by perforated ribs, the Nu_H-distribution is compared to that obtained with rib without perforation, which is named solid rib. The comparison relies on the evaluation of a local enhancement factor EF_h defined as the ratio of the heat transfer coefficient with porous and solid rib. Fig. 7 displays the downwind distribution of EF_h for the designs tested. The variation of the enhancement factor is plotted along different longitudinal paths (a, b, c) defined in Fig. 6. As sought for, the perforated turbulator improves significantly the heat transfer in the rear area. Depending on the turbulence promoter design, the enhancement zone may exceed a length of $4H$. After this distance the perforation effect is no more felt and the thermal behaviour is similar to that produced by the solid

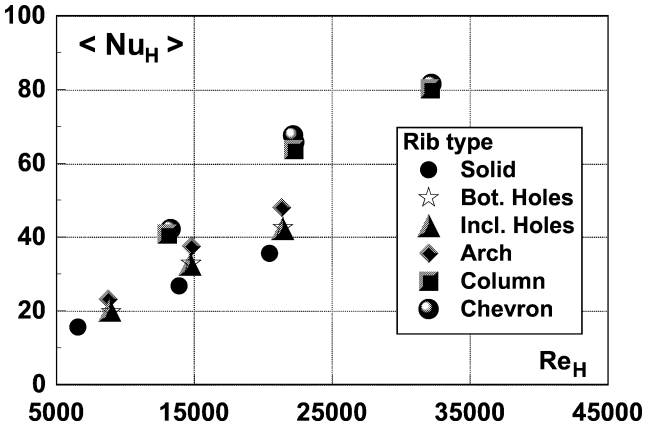

Fig. 8. Reynolds number effect on $\langle Nu \rangle$.

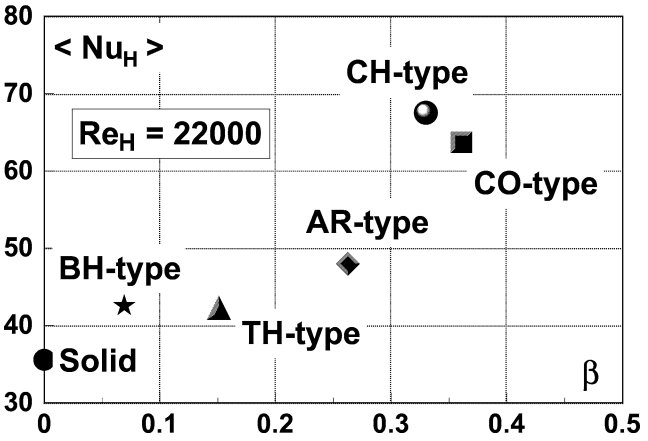

Fig. 9. Open-area ratio effect on $\langle Nu \rangle$.

rib. The maximum enhancement is located close to the back face of the rib ($x \leqslant H$) and may reach value as high as 3.

The comparative exercise is extended to the average Nusselt number $\langle Nu_H \rangle$ defined as the mean value over the area of observation (length of $4H$). Fig. 8 shows that $\langle Nu_H \rangle$ increases with the rib Reynolds number for all the turbulator designs. At the same flow conditions, the CO- and CH-type turbulators are the more thermal efficient: they afford about 65% of enhancement

An important design parameter of a perforated rib is the open-area factor β. It is the ratio of the clearance area to the total front area. Obviously, it is nil for solid-type rib. Since the larger is β the lower will be the pressure drop induced by the perforated ribs [5,8], it becomes worth plotting the average heat transfer coefficient $\langle Nu_H \rangle$ versus the surface porosity.

Fig. 9 compares all the perforated ribs tested. In the range of the investigated open-area ratio, 0 to 36%, the increase of β improves the heat transfer. Such a finding agrees with the data obtained on permeable ribs made of rows of circular perforations [4,7]. At more or less the same surface porosity and same Reynolds number (therefore at equivalent pumping power) the Chevron-type rib seems more efficient than the Column-type rib. To conclude on this aspect, the investigation has proceeded to experiments including ribbed wall with periodic perforated Chevron-type turbulators to highlight in particular the effect of the rib pitch.

4.2. Effect of rib spacing

Fig. 10 displays a typical sequential mapping of the Nusselt number *Nu* based on channel height and normalised by the corresponding smooth-channel value for $Re = 3200$, $\beta = 0.533$ and $P/H = 5$. The fully developed flow is reached after the 5th or the 6th rib. This finding is also obtained for all following tests performed for channel Reynolds number *Re* ranging from 10000 to 100000, open area factor β from 0.32 to 0.69 and pitch ratio P/H from 2 to 6. Thus, the data will focus on the heat transfer distribution in the 6th interval.

The effect of the pitch ratio P/H on the heat transfer distribution is depicted in Fig. 11. The increase of the P/H-value assists the flow penetration through the turbulators and improves the heat transfer. Part of the airflow passes through the perforated rib and interacts with the recirculation bubble generated behind the rib by the impingement of the upper free stream on the wall. As a consequence, the hot spot area occurring in the region just behind a solid-type rib does not exist anymore in presence of perforated turbulators and the local thermal enhancement factor may reach values as high as 3 as already underlined.

However, the plots of the average Nusselt number ratio reported in Figs. 12 and 13 indicate that the open area modulates this effect. At low β-values and/or small P/H, the system behaves like impermeable rib arrangement. At high β-values and/or large P/H, the turbulators do not suitably perturb the flow and the mean thermal enhancement factor $\langle Nu \rangle / Nu_o$ remains moderate. Therefore, it is not surprising to end at an optimal configuration that turns to be a pitch ratio of 5 for a surface porosity of about 0.53.

Finally, Fig. 14 emphasises the effect of the channel Reynolds number on the mean normalised Nusselt number. As the Reynolds number increases, the thermal exchange rises until a critical value at which the flow resistance due to surface porosity becomes too important. The air stream does not penetrate sufficiently through the permeable turbulator and the thermal efficiency declines. Therefore, an extremum exists depending on the open area factor. For the optimum configuration, the recommended values of Reynolds range from 30000 to 60000.

5. Conclusions

Steady-state heat transfer measurements behind two-dimensional perforated ribs immersed in a turbulent boundary layer are performed. Quantitative infrared thermography associated with the heated thin foil technique provides a detailed description of the thermal field. The mapping of

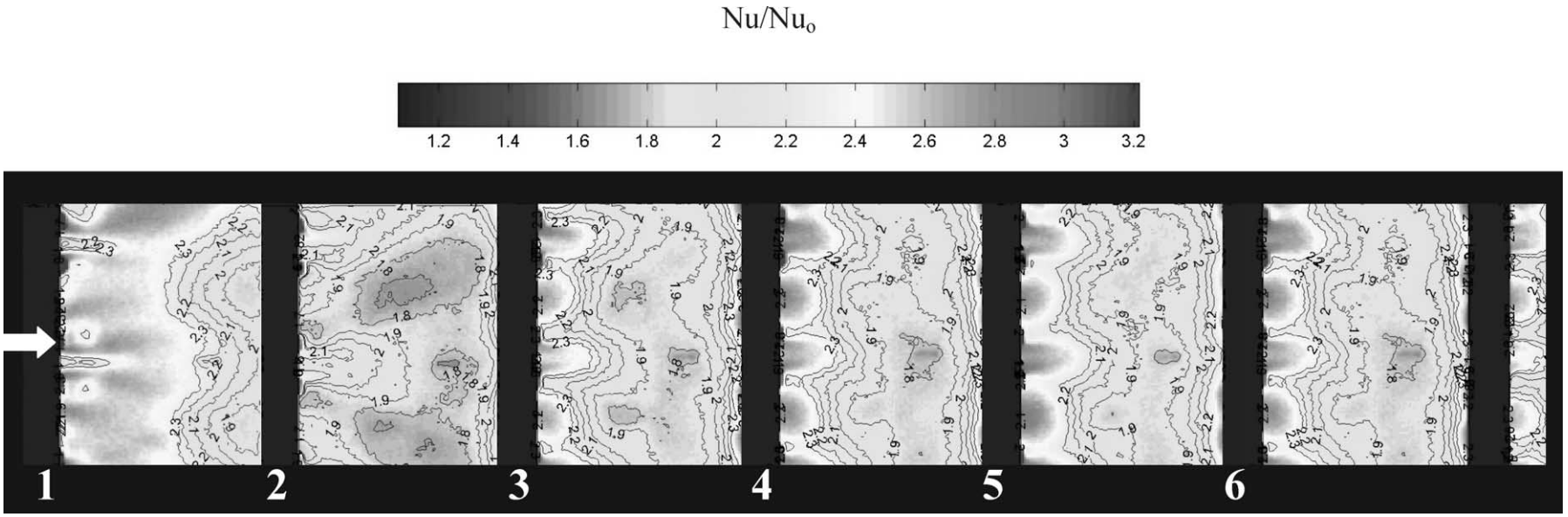

Fig. 10. Effect of the rib number on developed flow: Chevron type turbulator $Re = 32000$, $\beta = 0.533$, $P/H = 5$.

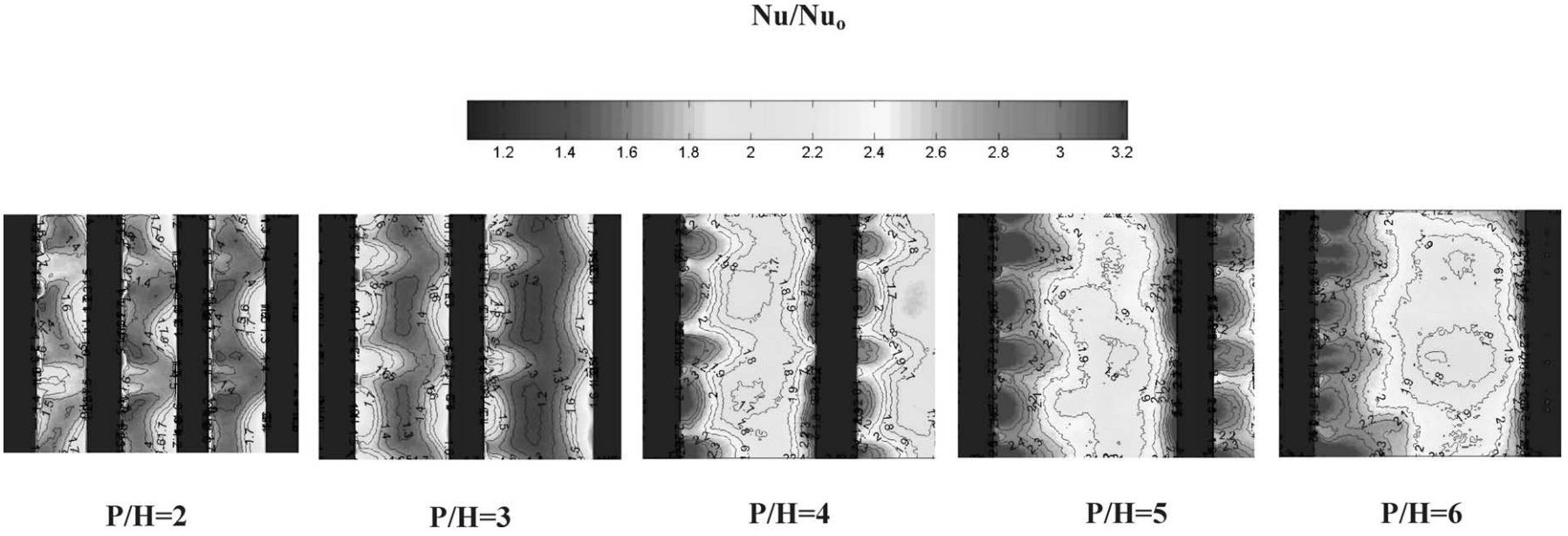

Fig. 11. Effect of the rib pitch ratio o the local heat transfer coefficient: $Re = 32000$, $\beta = 0.533$: Fully developed flow.

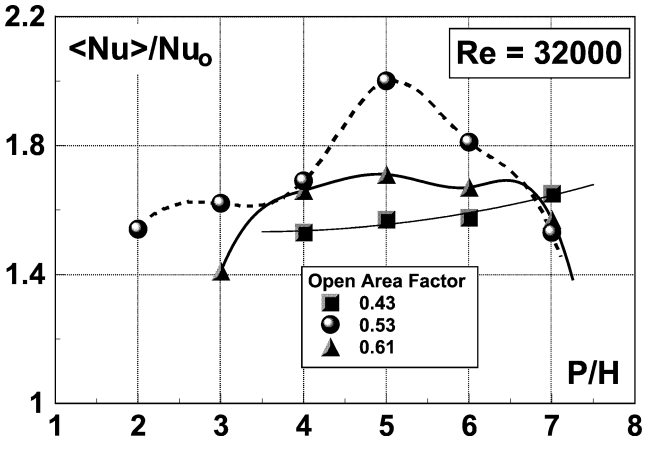

Fig. 12. Effect of the pitch ratio on the mean Nusselt number.

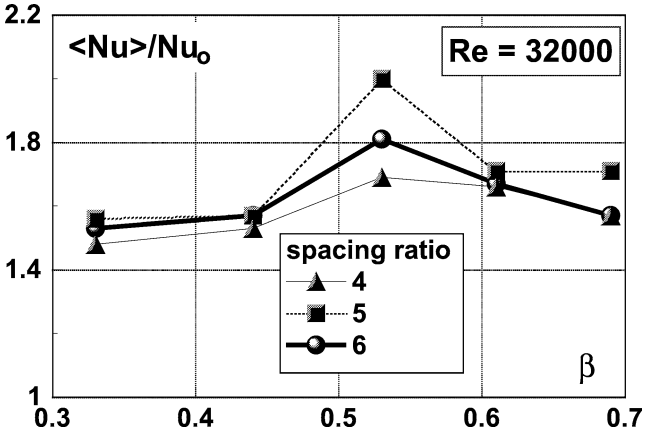

Fig. 13. Effect of the open area factor on the mean Nusselt number.

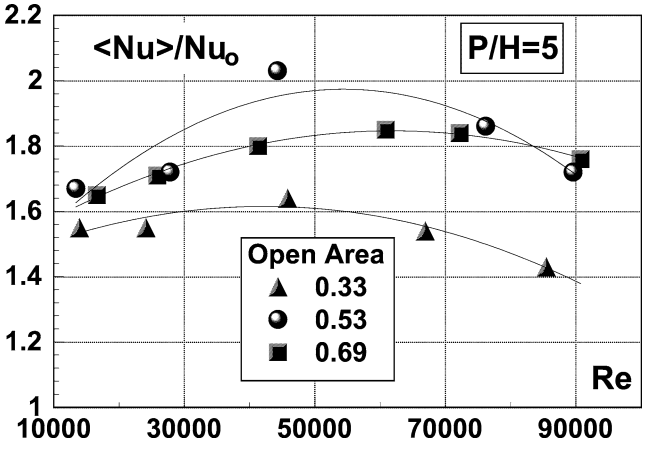

Fig. 14. Effect of the channel Reynolds number on the mean Nusselt number.

the heat transfer coefficient constitutes a useful visualisation support to interpret the complexity of the resulting flow.

In a first step, the study compares the average heat transfer coefficients obtained with five new designs of perforated turbulators. Part of the air flow passes through the perforated rib and interacts with the recirculation bubble generated behind the rib by the impingement of the upper free stream on the wall. As a consequence the hot spot area occurring in the region just behind a solid-type rib does not exist anymore in the corresponding region of the perforated turbulator. The local thermal enhancement factor of perforated ribs may reach peak value of 3.

The comparison of the average heat transfer coefficients obtained with the different turbulators indicates that the increase of the open-area ratio of the perforated rib up to 36% and for Reynolds number based of the obstacle height higher than 20000, improves significantly the heat exchange. Among the turbulators tested, the finding encourages further investigating a channel wall implemented with periodically chevron-clearance-type ribs. With such a type of perforated, turbulators, the fully developed flow is reached after 5 to 6 ribs and the optimal design combines a rib pitch ratio of 5 with an open area factor of 0.53. The recommended range of channel Reynolds number is from 30000 to 60000.

References

[1] J.R.C. Hunt, Flow Around Bluff Obstacles, VKI Lecture Series 1984-06, von Karman Institute for Fluids Dynamics, Rhode Saint Genèse, Belgium, 1984.

[2] J.-M. Buchlin, Heat transfer behind a rectangular cylinder in a boundary layer, Proceedings of the Workshop Advanced Infrared Technology and Applications, Atti Fond. G. Ronchi, Hermography 49 (1) (1993) 305–315.

[3] K. Ichimiya, Mitsushiro, Enhancement of the heat transfer of wide temperature range in a narrow flow passage (effects of porous-type turbulence promoters in normal temperature range), in: R.K. Shah, E.N. Ganic, K.T. Yang (Eds.), Proceedings of Experimental Heat Transfer, Fluid Mechanic, and Thermodynamics, Dubrovnik, Yugoslavia, 1988, pp. 659–664.

[4] J.J. Hwang, T.M. Liou, Augmented heat transfer in a rectangular channel with permeable ribs mounted on the wall, ASME J. Heat Transfer 116 (1994) 912–919.

[5] J.J. Hwang, T.M. Liou, Heat transfer and friction in a low-aspect-ratio rectangular channel with staggered perforated ribs on two opposite walls, ASME J. Heat Transfer 117 (1995) 843–850.

[6] T.M. Liou, S.H. Chen, Turbulent heat and fluid flow in a passage distributed by detached perforated ribs of different heights, Internat. J. Heat Mass Transfer 41 (1998) 1795–1806.

[7] J.J. Hwang, T.M. Liou, Heat transfer in a rectangular channel with perforated turbulence promoters using holographic interferomerty measurement, Internat. J. Heat Mass Transfer 38 (1995) 3197–3207.

[8] J.J. Hwang, T.Y. Lia, T.M. Liou, Effect of fences thickness on pressure drop and heat transfer in a perforated-fenced channel, Internat. J. Heat Mass Transfer 41 (1998) 811–816.

[9] J.-M. Buchlin, Thermography Application to Heat Transfer of Impinging Jets, VKI Lecture Series 1986-09 on Flow Visualization and Digital Image Processing, von Karman Institute for Fluids Dynamics, Rhode Saint Genèse, Belgium, 1986.

[10] J.-M. Buchlin, M. Meyers, Infrared thermography study of a confined impinging circular jet, in: D. Balageas, G. Busse, G.-M. Carlomagno (Eds.), Proceedings of Quantitative Infrared Thermography QIRT '96, (Eurotherm Seminar 50), Editions Européennes Thermique et Industrie, Stuttgart, Germany, 1996, pp. 159–164.